THESIS FOR THE DEGREE OF LICENTIATE OF ENGINEERING

Thermal modelling and control of lithium-ion batteries

For enhanced thermal safety and lifetime

Godwin K. Peprah

Department of Electrical Engineering
Chalmers University of Technology
Gothenburg, Sweden, 2024

Thermal modelling and control of lithium-ion batteries

For enhanced thermal safety and lifetime

Department of Electrical Engineering
Chalmers University of Technology
SE-412 96 Gothenburg, Sweden
Phone: +46 (0)31 772 1000

Printed by Chalmers Reproservice
Gothenburg, Sweden, September 2024

To God, myself, family and friends.

Abstract

The urgent need to reduce greenhouse gas emissions has thrust electrification to the forefront of sustainable solutions. Electric Vehicles (EVs), powered by lithium-ion batteries (LiBs), offer a promising pathway to reducing the transport sector's carbon footprint, which accounts for one-quarter of global CO_2 emissions. However, these LiBs, which suffer from the so-called "Goldilocks syndrome", exhibit complex nonlinear behaviour and their functionality is strongly influenced by temperature. This necessitates a sophisticated thermal management system capable of controlling the battery temperature within desired limits, regardless of operating conditions. The challenge lies in balancing the trade-off between minimising thermal gradients within the cell and maintaining a low average temperature rise. Achieving this balance requires an optimal combination of tab (terminal) and surface cooling methods to leverage their unique individual strengths.

In this thesis, we present a new modelling framework for battery cells of different geometries by integrating Chebyshev spectral-Galerkin method and model component decomposition. Consequently, a library of reduced-order computationally efficient two-dimensional battery thermal models is obtained, characterised by different numbers of states. The proposed models allow for the independent control of tab and surface cooling channels for improved thermal performance optimisation. Evaluations under real-world vehicle driving and cooling scenarios demonstrate that these models accurately predict the battery's spatially resolved temperature distribution with minimal errors. Remarkably, the one-state model proves to be both more accurate and computationally efficient than the widely studied and commercially utilised two-state thermal equivalent circuit (TEC) model. Consequently, the proposed model can readily replace the TEC model in existing battery management system applications for enhanced safety and lifetime management. As the developed models enable targeted cooling control to any side of the cell, they are particularly suitable for battery temperature estimation and control in complex cooling scenarios. Furthermore, using these models, the thesis formalises the optimal integration of tab and surface cooling strategies as an optimal control problem and solves it using the model predictive control (MPC) framework. The evaluation of the MPC scheme demonstrates superior thermal performance compared to conventional side and base battery cooling methods. Ultimately, our proposed model and optimal scheme not only enhance immediate

thermal performance but also address long-term concerns regarding battery lifespan, safety, and economic viability, representing a valuable advancement in EV battery thermal management.

Keywords: Battery thermal management system, control-oriented thermal modelling, spectral method, model predictive control, cooling control.

List of Publications

This thesis is based on the following publications and their extensions:

[A] **Godwin K. Peprah**, Torsten Wik, Yicun Huang, Faisal Altaf, Changfu Zou, "Control-oriented 2D thermal modelling of cylindrical battery cells for optimal tab and surface cooling". Published in 2024 *American Control Conference (ACC), Toronto, Canada.*

[B] **Godwin K. Peprah**, Yicun Huang, Torsten Wik, Faisal Altaf, Changfu Zou, "Thermal modelling of battery cells for optimal tab and surface cooling control". Submitted to *IEEE Transactions on Control Systems Technology.*

Other publications by the author, not included in this thesis, are:

[C] **Godwin K. Peprah**, Francesco Liberati, Faisal Altaf, Gilbert Osei-Dadzie, Alessandro Di Giorgio, Antonio Pietrabissa, "Optimal load sharing in reconfigurable battery systems using an improved model predictive control method". Published in 29th Mediterranean Conf. on *Control and Automation (MED)*, Puglia, Italy, 2021, pp. 979-984, doi: 10.1109/MED51440.2021.9480237.

Acknowledgments

I would like to express my deepest gratitude to my supervisors, whose guidance and support have been invaluable throughout my thesis journey. My special thanks go to my main supervisor, Associate Prof. Changfu Zou, whose unwavering dedication and commitment were evident as he graciously made time to assist me, even during his vacation days, ensuring the completion of my journal. The insightful discussions and constructive feedback from Prof. Torsten Wik, Dr. Faisal Altaf, and Dr. Yicun Huang have been instrumental in shaping my research, and I am truly grateful for their expertise and encouragement.

I also wish to extend my heartfelt appreciation to my family and friends for their unwavering prayers and emotional support. Their encouragement has been a source of strength and motivation, helping me navigate the challenges of this academic endeavour. Thank you all for being an integral part of this journey.

Acronyms

EV:	Electric vehicle
Li-ion:	Lithium-ion
LiB:	Lithium-ion battery
TEC:	Thermal equivalent circuit
FE(M):	Finite element (method)
FD(M):	Finite difference (method)
PDE:	Partial differential equation
2D:	two-dimensional
SEI:	Solid electrolyte interphase
BMS:	Battery management system
SoC:	State-of-charge
BTMS:	Battery thermal management system
PCM:	Phase change material
q:	heat generation
ECM:	Electrochemical model
DFN:	Doyle-Fuller-Newman
ODE:	Ordinary differential equations
EQM:	Equivalent circuit model
WRM:	Weighted residual method
SGM:	spectral-Galerkin method
WLTP:	Worldwide harmonised light vehicle test procedure

MPC:	Model predictive control
ISBC:	Integrated switched-battery cooling
DC:	Direct current
PWM:	Pulse width modulator

Contents

Part I

Overview

CHAPTER 1

Introduction

1.1 Motivation

Many a traveller to the Mediterranean these recent summer months could not have missed the intense heat waves that characterised their holidays. Such phenomena illustrating broader environmental shifts are not isolated; from devastating wildfires in Australia and the increasingly severe hurricanes experienced in the United States, the impacts of a warming planet are becoming more apparent.

Human activities, primarily the burning of fossil fuels, have led to a significant increase in atmospheric CO_2 concentrations, rising from about 280 parts per million (ppm) in the 1850s-1900s, the pre-industrial times, to over 420 ppm today [1]. This 50% increase in CO_2 levels has resulted in a global average temperature rise of approximately 1.2°C since that period. For perspective, the global average surface temperature in April 2024 was 15.03°C, which is 1.58°C warmer than the estimated average for the pre-industrial period [2]. This warming has led to various climate change impacts, including more frequent and intense heat waves, changes in precipitation patterns, and rising sea levels [3], [4]. These changes are expected to continue and poten-

tially intensify if greenhouse gas emissions are not significantly reduced, with projections suggesting a global temperature increase of 1.5°C by 2050 under current emission trajectories [5].

According to the United Nations [6], the transport sector, including cars, trucks, buses, aviation, and shipping, contributes approximately one-quarter of global greenhouse gas emissions. This is largely due to its heavy reliance on fossil fuels, which account for over 90% of the sector's energy consumption. At this current time t and in the foreseeable future, electrification emerges as the most promising resolution to address this significant environmental impact. This resolve towards electrification requires a combination of strong regulations, fiscal incentives, and significant infrastructure investments [7].

At the heart of this transition are electric vehicles (EVs), which offer a promising path to reducing emissions. However, the performance and efficiency of EVs are critically dependent on their battery packs, typically composed of lithium (Li)-ion cells. These Li-ion batteries (LiBs) exhibit complex nonlinear behaviour, and their functionality is strongly influenced by temperature. Temperature affects multiple aspects of the LiB, including safety, electrochemical processes, charge acceptance, round-trip efficiency, power and energy capability, and lifetime [8]. Consequently, the need for a sophisticated thermal management system [9] becomes apparent. This system should be capable of controlling the battery temperature to desired values regardless of operating conditions.

Subject to various thermal boundary conditions such as liquid or air convection [10], battery cells can be thermally controlled at different surfaces, including the electrical connection tabs (terminals), cell surfaces, or both [11]. Prior literature studies have investigated the impact of tab and surface cooling methods on battery thermal performance. Hunt *et al.* and Zhao *et al.* concluded in [12], [13] that surface cooling can maintain Li-ion pouch cells at a lower average temperature under high current rates than tab cooling. In a case study, these authors also demonstrated that using tab cooling rather than surface cooling extended the lifetime of a battery pack by three times. Similar results were achieved in [14], [15] for cylindrical Li-ion cells, where tab cooling was shown to reduce the internal temperature inhomogeneities by about 25%.

It is clear that both surface and tab cooling have their individual strengths and weaknesses. However, to the best of our knowledge, there is no battery

control framework in the state-of-the-art literature that systematically investigates the optimal integration of these two cooling methods for advanced battery temperature management.

Thermal equivalent circuit (TEC) models with lumped parameters have been extensively utilized for control-oriented modelling of batteries due to their ease of implementation and computational efficiency [16], [17]. However, lumped parameter TECs can only predict average and surface temperatures and their applicability is limited to cells with small Biot numbers. Physics-based models [18] result in partial differential equations governing the underlying heat diffusion. They can predict the spatially distributed temperature field throughout the cell but are typically implemented via computationally expensive numerical methods, such as finite element (FE) and finite difference (FD) methods, rendering them impractical for control purposes. Spectral methods [19], [20] are alternative numerical methods for finding solutions to PDEs. They belong to the class of weighted residual methods, and unlike FE and FD methods, they make use of global (rather than local) approximating functions in the discretization of the spatial domain, rendering them computationally efficient. With this benefit in mind, the spectral method based on the Galerkin approach is adopted to develop low-order two-dimensional (2D) thermal models for cylindrical cells in [21] and for pouch cells in [22]. However, these models do not allow independent and targeted cooling control of battery tabs and surfaces, preventing their use for optimally combining tab and surface cooling for battery thermal management.

This thesis bridges the identified research gap by addressing the research questions in the next section.

1.2 Research questions

- Can a unified thermal modelling framework be developed that accurately captures both surface and tab cooling effects while remaining applicable across various battery form factors and chemistries?
- Does a hybrid strategy offer superior thermal performance and lifetime extensions over traditional single-method cooling approaches?
- Can a control framework be designed to dynamically adjust the balance between tab and surface cooling based on real-time thermal states and

ambient conditions of the battery cells?

- How do the thermal performance and computational efficiency of the developed spectral-based model compare to traditional lumped parameter TEC models and PDE-based models?

1.3 Thesis contributions

Here, we present a comprehensive strategy that will enable us to address the questions outlined in Section 1.2. Fig 1.1 presents a visual overview of our research framework, illustrating the various work packages and research problems that have been or are planned to be investigated. This research is structured into two primary categories: battery thermal modelling and control, each with various sub-categories branching off to cover specific aspects of the work.

This thesis focuses on the thermal modelling aspect, highlighted in the left red box, along with its associated branches, which are shaded in brown. This area forms the core of our research efforts and is explored in-depth in the accompanying papers. While the thermal control component is still in progress, we do touch upon one aspect of it — the optimal coolant split scheme. This provides a glimpse into the potential applications and implications of our thermal modelling.

1.4 Thesis outline

The thesis is organised as follows.

- Chapter 1 provides an introduction and motivation for the research work.
- Chapter 2 presents a basic overview of LiBs and discusses how temperature impacts their operation.
- In chapter 3, the key ideas pertinent to battery thermal management systems are introduced.
- Chapter 4 delves into various aspects of LiB modelling, including a soft introduction to spectral methods via a toy problem.

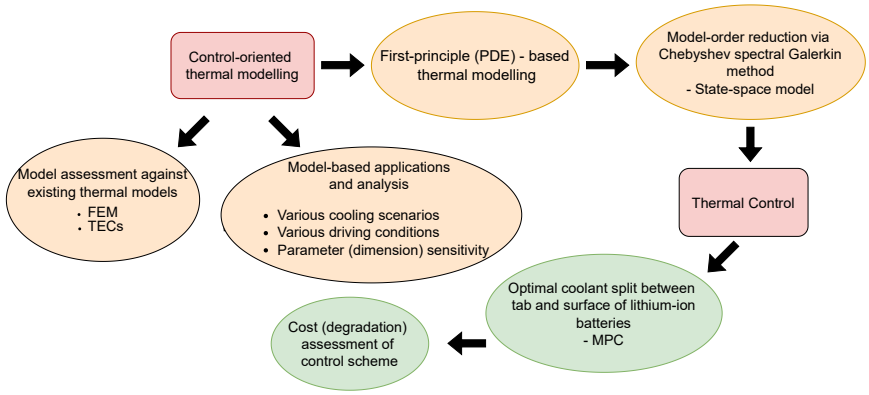

Figure 1.1: Overview map representing the project work packages. The two main project categories are shaded in red, while their sub-categories are represented in brown and green.

- Chapter 5 follows with a discussion on model-based applications of the proposed thermal model, with highlights on the thermal control aspects.
- Chapter 6 summarises the accompanying papers, while
- Chapter 7 concludes the thesis and explores potential future research directions.

CHAPTER 2

Lithium-ion batteries

A battery cell is the smallest electrochemical unit that generates voltage to power a load, with its nominal voltage determined by its chemical composition. Cells are classified based on rechargeability and power-to-energy ratio [23], [24]. Rechargeability divides them into primary (single-use) and secondary (rechargeable) cells. The power-to-energy ratio distinguishes between high-power cells, which have thin electrodes for efficient conduction, and high-energy cells, which have thick electrodes to store more active material. Due to these design differences, cells are typically optimized for either power or energy, but not both. A battery, often confused with a cell, is technically a combination of multiple cells connected in series or parallel. A battery module consists of multiple such combinations, and a battery pack is an assembly of several modules arranged to meet specific energy, power, and voltage requirements in EVs. For the purposes of this thesis, the terms battery and battery cell will be used interchangeably to simplify terminology, while acknowledging their technical distinctions.

2.1 Operating mechanisms

LiBs operate through the movement of Li-ions between the positive and negative electrodes, as illustrated in Fig. 2.1. During discharge, Li-ions move from the negative through the separator to the positive electrode. This ionic movement occurs via the electrolyte, which consists of lithium salt dissolved in an organic solvent. Simultaneously, electrons flow from the negative to the positive electrode through an external circuit, powering a connected load. During charging, an external power source reverses this flow [25], [26]. The negative

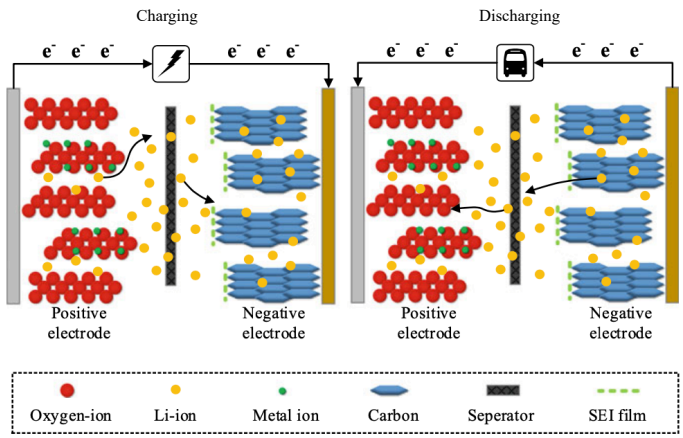

Figure 2.1: Basic structure and working principle of LiBs [27].

electrode is typically made of graphite, with newer variations incorporating silicon to enhance capacity. The positive electrode is commonly composed of metal oxides, such as nickel-manganese-cobalt (NMC), or lithium-iron-phosphate (LFP), which is a type of metal phosphate. A separator between the electrodes prevents short circuits while allowing Li-ions to flow freely [28]. The formation of the solid electrolyte interphase (SEI) [29] occurs on the surface of the negative electrode during the initial cycles of a LiB. The SEI layer forms due to electrolyte decomposition and functions to protect the electrode from further reactions with the electrolyte. While the SEI is essential for battery stability, its continuous growth and restructuring over time can lead to ageing, notably through capacity loss as the layer thickens, consuming active

Li and increasing cell impedance [30].

2.2 Temperature effects and safety

Few could have missed the recent media attention on LiBs due to safety concerns. Earlier this year in Melbourne, two students narrowly escaped a fire in their apartment after their LiB-powered mobile phone power bank exploded [31]. In 2022, multiple reports from India highlighted incidents where mopeds equipped with LiBs caught fire [32]. Similarly, Tesla's stock took a hit when several of their Model S EVs caught fire, and had to be recalled, with LiBs identified as the cause [33]. What do these cases have in common? The LiBs experienced thermal runaway.

Thermal runaway [34], [35] is a self-propagating, uncontrolled increase in temperature that causes conditions that lead to a further increase in temperature, creating a positive feedback loop. Fig. 2.2 illustrates the thermal runaway propagation cycle. In LiBs, it occurs when the heat generation rate exceeds the heat dissipation rate. This causes a rapid temperature rise, leading to a cascade of exothermic reactions and eventually to fire and explosion. Thermal runaway can be triggered by various factors, including overcharging, mechanical trauma which can lead to short circuits, or exposure to high ambient temperatures.

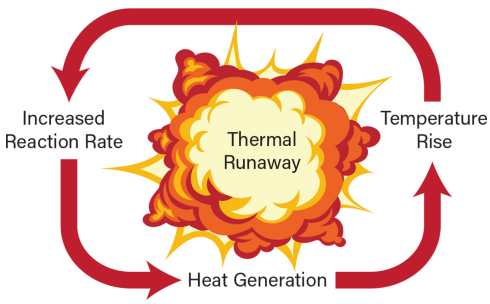

Figure 2.2: Thermal runaway cycle.

Operating batteries in extreme temperature conditions significantly affects their performance, lifespan, and safety. Figure 2.3 illustrates these effects. In cold environments, such as those in Scandinavia, low temperatures in-

crease electrolyte viscosity, reducing ionic conductivity, and increasing internal impedance. This results in decreased capacity and power output [36]. At subzero temperatures, the introduction of high currents may lead to Li plating. Li plating is the undesirable deposition of metallic Li on the negative electrode surface during charging, which can lead to the formation of needle-like structures called dendrites that may penetrate the separator, potentially causing short circuits and triggering thermal runaway [37]. Conversely, in hot climates like those in the tropics, elevated temperatures accelerate the growth of the SEI layer, leading to accelerated degradation. Additionally, the separator may rupture, and the electrolyte may decompose, creating the perfect initiating recipe for thermal runaway [38].

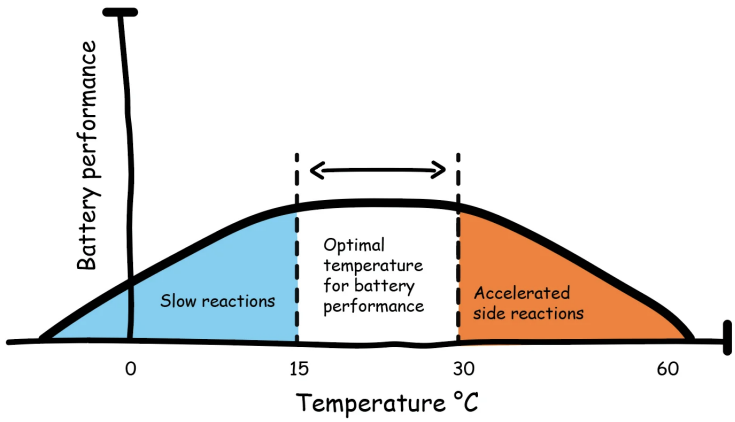

Figure 2.3: Optimum temperature range of LiBs [39].

Advances in battery design and thermal management systems are crucial for enhancing the safety and reliability of LiBs across various applications. Implementing efficient cooling and preheating strategies is key to maintaining optimal temperatures, and ensuring battery longevity, safety, and enhanced performance.

CHAPTER 3

Battery thermal management systems

LiB battery packs are invariably equipped with a battery management system (BMS), which functions as the intelligent brain of the pack. It integrates hardware and software components to monitor, control, and optimize battery performance [40]. Fig. 3.1 presents a general structure of a typical BMS. As battery technology has advanced, the BMS has evolved from a simple monitoring unit to a sophisticated, multi-functional system capable of executing complex algorithms and communicating with other vehicle systems [41]. Key functionalities of modern BMS include estimating critical battery states such as state-of-charge (SoC) [42], state-of-health [43], and state-of-power [44]. Additionally, BMS perform energy equalisation [45], fault diagnosis [46], and thermal management [9].

The battery thermal management system (BTMS) is particularly crucial for enhancing battery performance and safety. This aspect will be further explored in the subsequent sections.

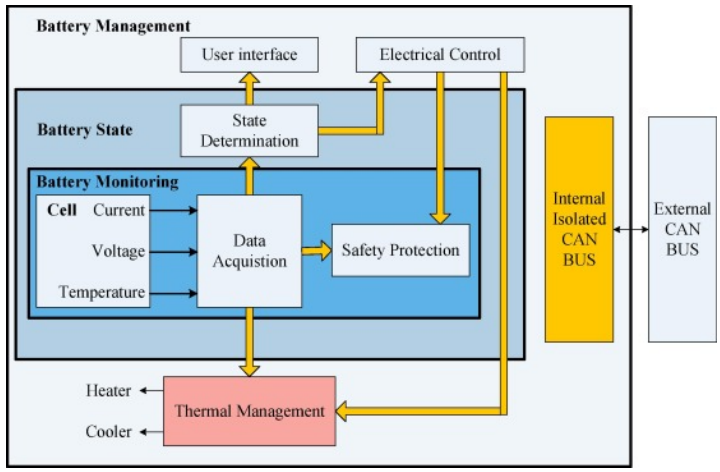

Figure 3.1: High-level BMS structure [47].

3.1 Battery cooling

During operation, LiBs generate heat due to internal resistance and electrochemical reactions, particularly under high power demands, fast charging, or discharging. Excessive heat can lead to thermal runaway, capacity degradation, and even catastrophic failure, making cooling a vital aspect of BTMS [9]. As shown in Fig 3.2, there are several cooling methods [9], [10], [48] employed in battery thermal management, each with its advantages and limitations. These methods can be broadly classified into passive, active, and hybrid cooling methods, with the cooling media being air, liquid, or some phase change materials.

Passive cooling utilizes natural convection and radiation to dissipate heat. It is simple and energy-efficient, suitable for applications with moderate heat generation. However, its effectiveness is limited under high thermal loads. Active cooling involves forced convection through the use of fans and/or pumps to enhance heat dissipation. Lastly, hybrid systems integrate passive and active cooling methods for optimal thermal performance. We explore below a few cooling methods in the state-of-the-art, namely, air, liquid, phase change material (PCM), heat pipe, and refrigeration cooling.

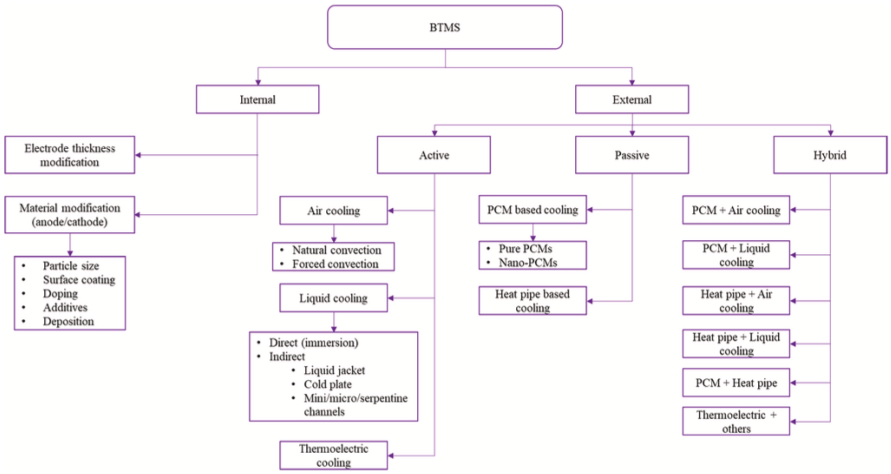

Figure 3.2: BTMS classification [49].

Air cooling

Air cooling [50] is often used due to its simplicity and cost-effectiveness. However, air cooling is generally less efficient and may not be sufficient for high-power applications or densely packed battery cells. This is due to air's low thermal conductivity compared to other heat transfer media such as liquid. This method can either be passive, active, or combined with other methods in a hybrid scheme to enhance battery heat dissipation. Fig 3.3 illustrates a simple air cooling system.

Liquid cooling

Liquid cooling [52] provides superior thermal management compared to air cooling. This method operates by circulating a coolant, such as water or glycol-based fluid through the battery pack. Due to the higher thermal conductivity of liquids, heat is removed more effectively even under high-stress conditions of high ambient temperatures or rapid battery cycling. Liquid cooling can be designed with the coolant in direct contact with battery cells or indirectly with the coolant circulating through channels or cooling plates adjacent to the cells. The latter is more common due to its safety and ease of

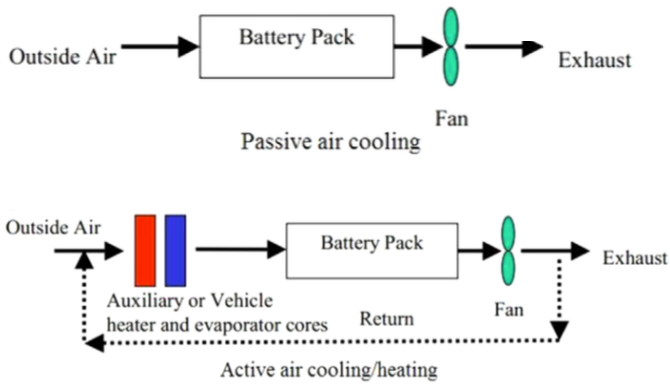

Figure 3.3: Air BTMS [51].

maintenance. A simple liquid cooling system is illustrated in Fig 3.4.

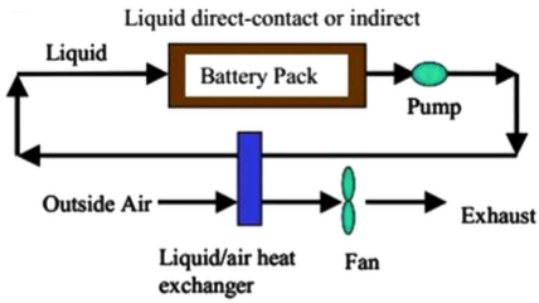

Figure 3.4: Liquid BTMS [51].

PCMs

Owing to its high latent heat, PCMs [53] can absorb enormous amounts of heat produced by LiBs as the materials change phase, typically from solid to liquid. This method is an effective passive cooling method, providing thermal

regulation without the need for moving parts. PCMs can be integrated into battery modules to absorb heat during high-load operations. However, the relatively low thermal conductivity of PCMs and the challenge of dissipating heat over extended periods limit its application. Most literature studies on PCMs mainly focus on improving the thermal conductivity of pure paraffin PCM by using additives such as metal foams, metal fins and expanded graphite to form composite PCMs. Fig 3.5 shows a battery module surrounded by pure paraffin PCM.

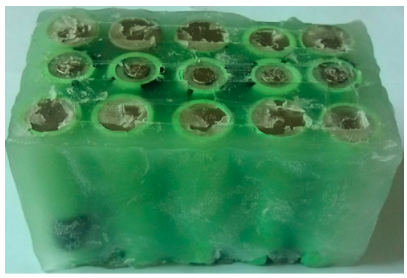

Figure 3.5: A battery module embedded in pure paraffin [54].

Heat pipes

Heat pipes [55] are passive cooling methods that use the principles of phase change to transfer heat from the battery cells to a heat sink or the environment. They have a super-high thermal conductivity making them highly efficient. They can also be integrated into battery packs to manage localized hotspots. Their lightweight and compact nature makes them suitable for EV applications, where space and weight are constraints. Fig 3.6 illustrates the working principle of a heat pipe.

Refrigeration

Refrigeration [48], [56] is an active cooling method that has garnered a lot of research attention in recent years due to it being the most effective method for maintaining low operating temperatures, especially in high-power applications or in hot climates. It uses phase change material in a refrigeration cycle to actively cool the battery pack. However, refrigeration systems are complex

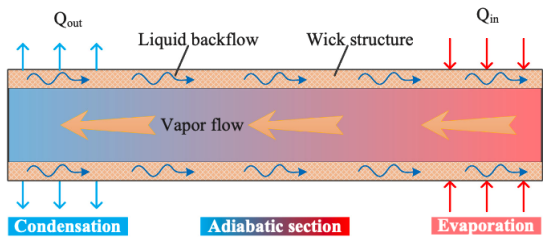

Figure 3.6: Working principle of the heat pipe [47]. It functions through three sections: evaporation, adiabatic, and condensation. The working fluid evaporates when exposed to high temperatures, carries the heat to the condensation section, where it releases the heat and condenses, completing the cycle.

and costly, making their adoption in EVs a bit measured.

Selecting the appropriate cooling strategy depends on several factors, including the specific application, battery pack design, cost, and environmental conditions. As battery technologies continue to evolve, so will cooling methods.

3.2 Low-temperature battery heating

Low-temperature battery heating is essential for maintaining the performance and safety of LiBs in cold environments [36]. At subzero temperatures, battery performance deteriorates due to reduced electrochemical reaction rates and the risk of Li plating, which can lead to operational difficulties and safety hazards in EVs [57]. To address these issues, various battery preheating strategies have been developed and can be categorized into external and internal methods, as illustrated in Fig 3.7.

External heating

External heating [57], [58] involves transferring heat from an external source to the battery using convective or conductive methods. This can include air, liquid, heat pump systems, and resistance or Peltier-effect heating [59]. While effective, external methods can suffer from long warm-up times and

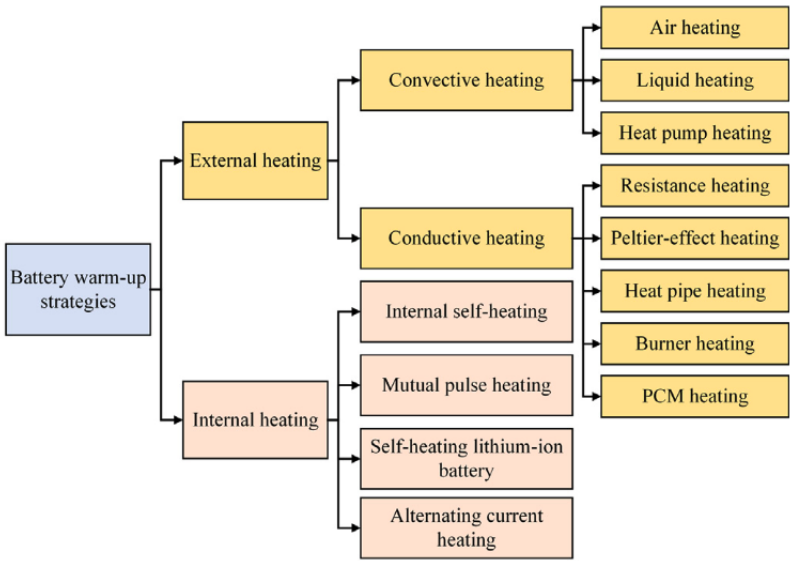

Figure 3.7: Existing preheating strategies [58].

energy inefficiencies due to heat loss. Fig 3.8 illustrates an example of external heating.

Internal heating

Internal heating [57] leverages the battery's electrical resistance to generate heat by applying a current, thereby warming the battery from within. This approach can be more efficient and quicker than external methods but requires careful management to minimize battery degradation. Recent innovations, such as self-heating LiBs [60] and alternating current heating [61], aim to optimize the balance between heating efficiency and battery health. An example of internal heating is illustrated in Fig 3.9.

Heating strategies are part of broader BTMS designed to optimize battery performance across different temperatures and usage conditions.

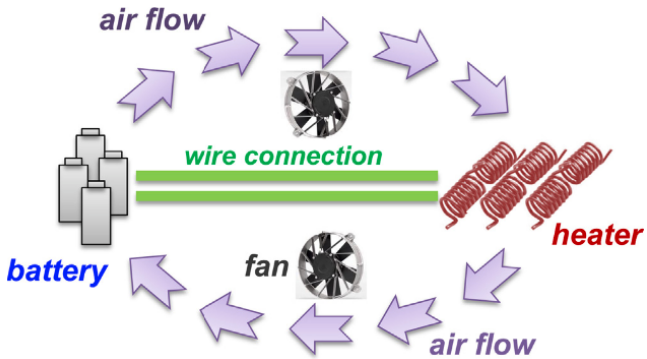

Figure 3.8: Convective battery heating [57].

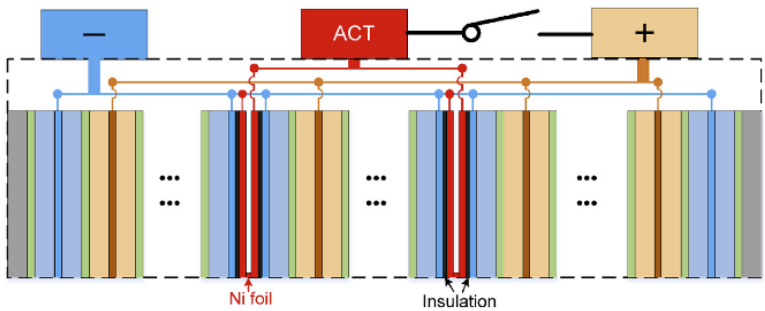

Figure 3.9: Self-heating LiB with multiple Nickel (Ni) foils inserted [60]. The Ni foils are strategically inserted within the battery structure to facilitate efficient heat generation and distribution. ACT is an activation switch that closes the heating circuit.

CHAPTER 4

Battery Modelling

In academia and industry, the mathematical modelling of battery cells, regarded as multidisciplinary, has long been recognised as an important yet difficult problem. The complexity arises from the electrochemical reactions [62] occurring within the cells, which are influenced by numerous factors and uncertainties. These reactions and the associated electrical and thermal processes exhibit strong time variations and nonlinear behaviour, making accurate modelling non-trivial.

Battery models are essential for understanding and predicting the behaviour of batteries under various operating conditions. These models typically involve two key aspects, i.e., electrical and thermal [62]. The electrical model captures the behaviour of the battery in terms of voltage, current, and SoC, while the thermal model describes the heat generation [63], [64] and temperature distribution within the battery. These two aspects are tightly coupled, as the electrochemical reactions that govern the electrical behaviour also generate heat, which affects the cell's temperature-dependent reaction rates and other properties.

Heat generation in batteries

Heat generation [63], [65], [66], q, in batteries, can be classified into reversible and irreversible components and primarily arises from three sources. Namely,

- joule heating, also known as ohmic losses. This irreversible component of q is the resistive heating due to the current flow through the battery's internal resistance. The rate of heat generation due to joule heating is defined as
$$q_j = I^2 R, \tag{4.1}$$
where I is the current flowing through the battery, and R is the battery's internal resistance.

- reaction heat, which is the heat generated or absorbed due to electrochemical reactions occurring within the battery. This q is primarily regarded as reversible, however, if the enthalpy change includes contributions from irreversible processes such as side reactions and other inefficiencies within the cell, then the reaction q would be classified as irreversible. The reaction q denoted here as q_r can be quantified using enthalpy change of the reaction,
$$q_r = \frac{\partial G}{\partial T} I, \tag{4.2}$$
where G is the Gibbs free energy and T is the temperature.

- entropy heat, a reversible form of q, is associated with the entropy change during the charge and discharge process. The entropy change per unit charge transferred is expressed as
$$q_e = \frac{\partial S}{\partial T} IT, \tag{4.3}$$
where S is the entropy of the system.

The total q within a battery is the sum of (4.1)–(4.3), namely, there exist

$$q = q_j + q_r + q_e. \tag{4.4}$$

In many practical modelling scenarios, some of these q components are often simplified or ignored to reduce complexity. For instance, q_e is frequently

neglected in models when the temperature variations within the battery are relatively small, as its contribution becomes negligible compared to q_j. These simplifications are typically valid in steady-state conditions or during low-rate cycling, where the thermal effects are less pronounced.

The following sections delve into various approaches to battery modelling, starting from first principles to more empirical and grey-box methods, while also considering the numerical methods used for solving the associated partial differential equations (PDEs).

4.1 First-principles modelling

First-principles modelling [67] of LiBs involves a detailed representation of the physical and chemical processes occurring within the battery cells. This approach is often rooted in fundamental laws of physics and chemistry, such as the conservation of mass, charge, and energy. The models typically capture the electrochemical reactions, ion transport, and thermal dynamics within the battery. These models can predict the battery's internal states, such as species concentration, electric potential distribution, and temperature profile. The complexity of first-principles models makes them computationally intensive but highly accurate, making them ideal for in-depth battery studies and analysis.

Electrochemical modelling

Electrochemical models (ECMs) [62], [68], [69] focus on describing the internal processes of the battery at the microscopic level, including the intercalation and de-intercalation of Li-ions, the associated charge-transfer reactions, and the transport of ions through the electrolyte. The most common ECM is the Doyle-Fuller-Newman (DFN) model [70], based on porous electrode theory. The DFN model uses a set of coupled PDEs to capture the intercalation kinetics of Li-ions within electrode particles, electrolyte dynamics, and electric potentials in the electrodes. The key DFN equations include the solid phase electric potential, ϕ_s, governed by Ohm's Law,

$$\nabla \cdot (\sigma \nabla \phi_s) = -a_s i, \tag{4.5}$$

where ∇, σ, a_s, and i are the gradient, electronic conductivity of the electrode material, specific interfacial area, and current density due to electrochemical reactions, respectively. The electrolyte phase potential, ϕ_e,

$$\nabla \cdot (\kappa \nabla \phi_e) = a_s i, \tag{4.6}$$

where κ represents the ionic conductivity of the electrolyte. Li concentration in solid particles, c_s, governed by the diffusion equation

$$\frac{\partial c_s}{\partial t} = \frac{1}{r^2}\frac{\partial}{\partial r}\left(r^2 D_s \frac{\partial c_s}{\partial r}\right), \tag{4.7}$$

where D_s and r are the diffusion coefficient of Li-ions in the electrode material, and radial coordinate within spherical particles, respectively. The Li concentration in electrolyte, c_e,

$$\epsilon_e \frac{\partial c_e}{\partial t} + \nabla \cdot F = a_s i, \tag{4.8}$$

where ϵ_e and F are the porosity of the electrode and molar flux of Li-ions in the electrolyte, respectively. Lastly, the electrode-electrolyte interfacial current density, represented by the Butler-Volmer equation

$$i = i_0 \left[\exp\left(\frac{\alpha_a F_a}{R_u T}(\phi_s - \phi_e - U)\right) - \exp\left(-\frac{\alpha_e F_a}{R_u T}(\phi_s - \phi_e - V_{ocv})\right)\right], \tag{4.9}$$

where i_o is the exchange current density, which depends on material properties and SoC, α_a and α_e are the anodic and cathodic transfer coefficients, respectively. F_a, R_u, T, and V_{ocv} are Faraday's constant, the universal gas constant, absolute temperature, and the open circuit potential, which is a function of SoC and material properties.

PDE-based thermal modelling

The heat conduction within the battery is typically modelled by the parabolic PDE heat equation [71],

$$\rho C_p \frac{\partial T}{\partial t} = \nabla \cdot (k \nabla T) + q, \tag{4.10}$$

where ρ, C_p, and k are the battery density, specific heat capacity, and thermal conductivity, respectively. Assuming k is constant (homogenous material) for simplicity, the first term on the right-hand side of (4.10) becomes

$$\nabla \cdot (k\nabla T) = k\nabla^2 T, \tag{4.11}$$

where ∇^2 is the Laplacian of the temperature T, which in a three-dimensional Cartesian coordinate system (x, y, z) is given by

$$\nabla^2 T = \frac{\partial^2 T}{\partial x^2} + \frac{\partial^2 T}{\partial y^2} + \frac{\partial^2 T}{\partial z^2} \tag{4.12}$$

Equation (4.10) represents the balance between heat accumulation, conduction, and generation.

First-principles models such as (4.5)–(4.12) require appropriate boundary and initial conditions to solve them, typically via numerical methods.

4.2 Phenomenological and grey box modelling

In contrast to fundamental models discussed in Section 4.1, phenomenological [72] and grey box [73]models use empirical data to infer system behaviour without fully describing the underlying physics. These models provide the input-output relationship of the cell, often using lumped parameters. Lumped parameter modelling [62], [74] simplifies the behaviour of spatially distributed systems into discrete entities, approximating the behaviour of these systems under specific assumptions. With grey box models, input-output experimental data is fitted to a parameterized model with a known structure using lumped parameters. Grey box models combine elements of white box models, like fundamental models, with black box models. Black box battery models [62], [75] are typically data-driven, employing machine learning approaches to identify parameters to describe the relationship between some input variables and their corresponding outputs.

While phenomenological models are generally less accurate than their first-principles counterparts due to their inability to account for cell behaviour across all operating regions in their basic form, they are less complex and often represented by ordinary differential equations (ODEs). This simplicity makes them computationally more efficient and well-suited for real-time control and

estimation applications, which is why they are widely used in commercial BMS. The most common battery models in this category include equivalent circuit models (EQM) and thermal equivalent circuit (TEC) models.

Equivalent circuit modelling

EQMs [16], [74] represent the battery using electrical components like resistors, capacitors, and voltage sources, to simulate the battery's response under different operating conditions. Fig. 4.1 illustrates examples of two EQMs comprising n-resistor capacitor (RC) networks, commonly referred to as the Randle model, where n denotes the number of RC branches. These branches represent the polarisation and diffusion effects within the cell. Using the Thevenin EQM as an example, the input-output relationship of the EQM is derived based on Kirchhoff's voltage and current law as follows,

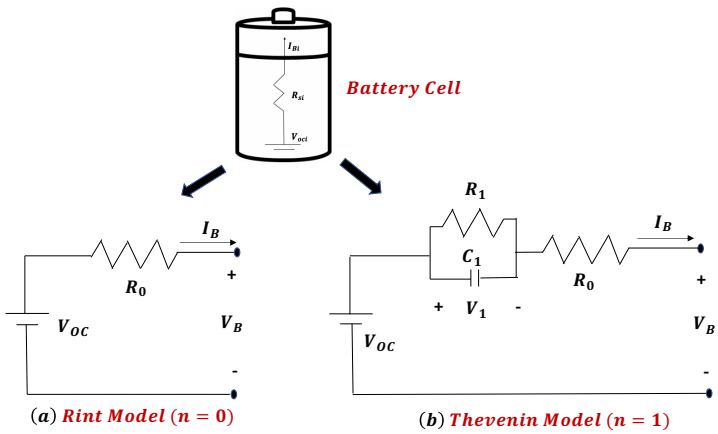

Figure 4.1: Special cases of the Randle EQM. (a) Rint EQM with no RC branch. (b) Thevenin EQM with 1 RC branch.

$$\dot{Z} = -mI_B \tag{4.13a}$$

$$\dot{V}_1 = -\frac{V_1}{R_1 C_1} + \frac{I_B}{C_1}, \tag{4.13b}$$

$$V_B = V_{oc} - V_1 - I_B R_0, \tag{4.13c}$$

where $Z \in [0,1]$, V_{oc}, V_B, R_0, and I_B are the normalised SoC, open-circuit voltage, terminal voltage, and internal resistance, respectively. V_1, R_1, and C_1 are the polarization voltage, resistance, and capacitance of the RC network, respectively. $m = 1/3600Q$ with Q being the coulomb capacity.

Thermal equivalent circuit modelling

TEC models [16], [17], [65], [76] represent the thermal behaviour of the battery using lumped components analogous to those in EQMs, such as thermal resistors that represent resistance to heat flow and thermal capacitors that represent heat storage capacity. TEC models often assume a uniform temperature distribution within each lumped component. This assumption is valid when the Biot number [71],

$$Bi = \frac{hL}{k}, \tag{4.14}$$

is much less than 1, indicating that the internal thermal resistance is negligible compared to the resistance at the heat transfer boundary. In (4.14), h, L, and k are the convective heat transfer coefficient, characteristic length, and thermal conductivity of the battery. This assumption simplifies the model to a single temperature node per component. TECs also assume linear and time-invariant system properties, instantaneous thermal responses, and often simplified boundary conditions, making them computationally efficient but potentially less accurate in complex, real-world scenarios. The TEC model shown in Fig 4.2 has been extensively studied in the literature [16], [17] and features lumped parameters and two states in the form

$$C_c \dot{T}_c(t) = q(t) + \frac{T_s(t) - T_c(t)}{R_c}, \tag{4.15a}$$

$$C_s \dot{T}_s(t) = \frac{T_f - T_s(t)}{R_u} + \frac{T_s(t) - T_c(t)}{R_c}, \tag{4.15b}$$

where T_c, T_s, and T_f represent the core, surface and ambient temperatures, respectively. R_c is the heat conduction resistance, which quantifies the heat exchange between the core and surface. R_u is the convection resistance, which measures the convection cooling along the battery surface and depends on the pack geometry, coolant type, and flow rate. C_c and C_s denote the core and surface (casing) heat capacity, respectively.

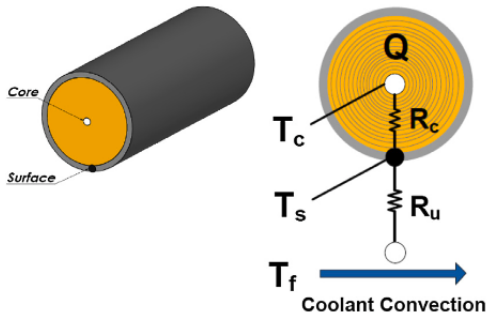

Figure 4.2: Two-state TEC model [17].

In the accompanying paper B, we evaluated the efficacy and applicability of our developed model against (4.15). Our findings indicate that, unlike our model, the TEC model is unreliable for predicting the local thermal behaviour and may be limited to applications with only small heat generation in the battery cell. Additionally, we examined the computational times of our proposed model across various states and compared them with that of the TEC model. We concluded that our model even with only one state is more efficient than its TEC counterpart, achieving a 28.7% reduction in computational time. Models with higher orders also maintained computational times within the same order of magnitude as the TEC model. These results suggest that our model can readily replace (4.15) in existing BMSs to improve battery thermal performance in the real world.

4.3 Numerical solutions of PDE-based thermal models

Numerical methods are essential for solving PDE models, especially when these models involve complex boundary conditions and spatially varying properties that are difficult to handle analytically [77]. These methods are generally categorized into local and global approaches. The finite difference (FDM) and finite element methods (FEM) are based on local arguments, whereas the spectral method is global in character [19], [77].

In practice, FEM is particularly well-suited for handling problems with

complex geometries and varying material properties, whereas spectral methods offer superior accuracy, at the expense of domain flexibility [19]. FEM and spectral methods are used to discretize and solve PDE-based battery thermal models, providing insights into the temperature distributions and heat flows within the battery under various operating conditions.

Finite element methods

FEM [78], [79] is a powerful numerical technique used to obtain approximate solutions to boundary value problems for PDEs. FEM partitions the problem domain into smaller subdomains, called finite elements, which are interconnected at points known as nodes.

In FEM, Lagrange polynomials [78] are commonly used as basis functions for approximating the solution within each element. These polynomials vary from simple linear to higher-order polynomials depending on the complexity and accuracy requirements of the problem. With the spatial variable x, the general form for Lagrange polynomials $N_i(x)$ in an element with n nodes is given by,

$$N_i(x) = \prod_{j=1, j\neq i}^{n} \frac{x - x_j}{x_i - x_j}. \tag{4.16}$$

For a linear element, i.e., $n = 2$, (4.16) reduces to

$$N_1(x) = \frac{x - x_2}{x_1 - x_2}, \qquad N_2(x) = \frac{x - x_1}{x_2 - x_1}. \tag{4.17}$$

These polynomials are designed such that

$$N_i(x_j) = \delta_{ij}, \tag{4.18}$$

where δ_{ij} is the Kronecker delta, which means each polynomial is 1 at its node and 0 at all others of the element.

Despite its many strengths, FEM is not typically suited for real-time battery control applications due to its computationally intensive nature. The detailed meshing of complex geometries and the iterative solving of large systems of equations demand substantial computational resources and processing time, which limits its practicality for dynamic, real-time scenarios. This limitation is a key reason why alternative methods, such as spectral methods, are considered in this thesis for more efficient real-time analysis.

Spectral methods

Spectral methods [19], [20] are another class of numerical techniques used for solving PDEs. They belong to the family of weighted residual methods (WRMs), which form the basis of many numerical methods including FEM, spectral, and finite volume. WRMs represent a particular group of approximation techniques, which focus on minimizing residuals (or errors) in a systematic way, leading to specific formulations such as Galerkin and collocation methods. Spectral methods are particularly known for their high accuracy, especially when applied to problems with regular geometries and smooth solutions.

A key feature that sets spectral methods apart from FEM and FDM is the choice of trial (basis) and test functions. Spectral methods use globally smooth functions as trial and test functions [19]. Commonly employed functions include trigonometric functions or orthogonal polynomials which include Fourier, Chebyshev, Legendre, Laguerre and Hermite. The choice of the test functions defines the type of spectral method. For instance, in the spectral-Galerkin method (SGM), the test functions are the same as the trial ones, whereas, in the spectral-collocation method, the test functions are the Lagrange polynomials wherein the residuals are forced to zero at a set of preassigned collocation points.

In this thesis, the SGM based on Chebyshev orthogonal polynomials is used to develop a lower-order 2D thermal model for the cylindrical and pouch battery cells. The detailed methodology and results are presented in the accompanying papers A and B. For the benefit of the reader who might not be conversant with the SGM, we introduce the solution process for a toy problem, namely, the 1D heat equation of (4.10)–(4.12) here.

Model reduction of the 1D heat equation using Chebyshev SGM

The governing 1D heat equation in Cartesian coordinates is given by

$$\rho C_p \frac{\partial T(\tilde{x},t)}{\partial t} - k\frac{\partial^2 T(\tilde{x},t)}{\partial \tilde{x}^2} - q(t) = 0, \tag{4.19}$$

where t is time and $\tilde{x} \in [-1, 1]$ is the position coordinate. The convection boundary conditions are given by

$$k\frac{\partial T}{\partial \tilde{x}} = h\,(T - T_\infty) \quad \text{at } \tilde{x} = 1, \tag{4.20a}$$

$$k\frac{\partial T}{\partial \tilde{x}} = -h\,(T - T_\infty) \text{ at } \tilde{x} = -1, \tag{4.20b}$$

where h is the convection coefficient at the domain boundaries and T_∞ is the ambient fluid free-stream temperatures.

The starting point of the SGM is to approximate the solution of T in (4.19) by a finite sum

$$\hat{T}(\tilde{x}, t) = \sum_{n=1}^{N} c_n(t)\phi_n(\tilde{x}) + T_\infty, \tag{4.21}$$

where c_n are unknown expansion (solution) coefficients, and ϕ_n is the n-th Chebyshev basis (trial) function that must satisfy the boundary conditions of (4.20). N is the number of Chebyshev basis functions, and $n \in \{1, \cdots, N\}$. N represents the order of the system, also referred to as the number of states. It is a tuning parameter that depends on the required resolution of the model.

Let $P_n(\tilde{x}) = \cos(n\theta)$, with $\theta = \arccos(\tilde{x})$. Here, $P_n(\tilde{x})$ represents the Chebyshev polynomials of the first kind, of degree n. In spectral methods, to enable efficient solution computations and satisfaction of boundary conditions, neighbouring orthogonal polynomials should be used to form the basis functions. Therefore, we seek the basis functions as a compact combination of Chebyshev polynomials in the form [19]

$$\phi_n(\tilde{x}) = P_n(\tilde{x}) + a_n(\tilde{x})P_{n+1}(\tilde{x}) + b_n(\tilde{x})P_{n+2}(\tilde{x}), \tag{4.22}$$

where the coefficients a_n and b_n are defined according to Lemma 4.3 of [19].

Substituting (4.21) for T into (4.19) yields the residual denoted by R

$$R = \rho C_p\frac{\partial \hat{T}}{\partial t} - k\frac{\partial^2 \hat{T}}{\partial \tilde{x}^2} - q \neq 0, \tag{4.23}$$

The principle of the CSG method is to force an integral of the resulting residual R to zero as

$$\langle R, \eta \rangle = \left\langle \left[\rho C_p\frac{\partial \hat{T}}{\partial t} - k\frac{\partial^2 \hat{T}}{\partial \tilde{x}^2} - q\right], \eta \right\rangle = 0, \tag{4.24}$$

where we use the notation $\langle f, \eta \rangle$ to represent the inner product of f and a test function η in the domain, namely $\langle f, \eta \rangle = \int_{-1}^{1} f(\tilde{x})\eta(\tilde{x})d\tilde{x}$. For the SGM, the test function η must belong to the same set of Chebyshev basis functions, thereby giving $\eta = \phi_n$.

Substituting (4.24) with the actual form of $\hat{T}$, we have

$$\langle R, \eta \rangle = \left\langle \left[\rho C_p \frac{\partial \sum_{n=1}^{N} c_n(t)\phi_n}{\partial t} - k \frac{\partial^2 \sum_{n=1}^{N} c_n(t)\phi_n}{\partial \tilde{x}^2} - q \right], \eta \right\rangle = 0. \quad (4.25)$$

Finally, rewriting (4.25) in matrix-vector notations gives

$$\left\langle \left[\rho C_p [\phi_1, \cdots, \phi_N] \begin{bmatrix} \dot{c}_1(t) \\ \vdots \\ \dot{c}_N(t) \end{bmatrix} - k \left[\frac{\partial^2 \phi_1}{\partial \tilde{x}^2}, \cdots, \frac{\partial^2 \phi_N}{\partial \tilde{x}^2} \right] \begin{bmatrix} c_1(t) \\ \vdots \\ c_N(t) \end{bmatrix} - q \right], \eta \right\rangle = 0. \quad (4.26)$$

Equation (4.26) can be written in the compact form as

$$G\dot{X}(t) = AX(t) + Bu(t), \quad (4.27a)$$
$$Y(t) = CX(t) + Du(t), \quad (4.27b)$$

where the states, inputs and system matrices are given by

$$X = [c_1, \cdots, c_N]^T, \quad (4.28a)$$
$$u = [q \ T_\infty]^T, \quad (4.28b)$$
$$G = \rho C_p \langle \phi_n, \eta \rangle, \quad (4.28c)$$
$$A = k \left\langle \frac{\partial^2 \phi_n}{\partial \tilde{x}^2}, \eta \right\rangle, \quad (4.28d)$$
$$B(:, 1) = \langle q, \eta \rangle, \quad (4.28e)$$
$$B(:, 2) = 0. \quad (4.28f)$$

Choosing the temperatures at the left and right boundaries, $T(\tilde{x} = -1)$ and

$T(\tilde{x}=1)$ as the outputs of the system, we have

$$Y = \begin{bmatrix}\hat{T}(-1,t) & \hat{T}(1,t)\end{bmatrix}^T, \tag{4.29a}$$

$$C(1,:) = \phi_n(-1), \tag{4.29b}$$

$$C(2,:) = \phi_n(1), \tag{4.29c}$$

$$D = \begin{bmatrix}0 & 1\\ 0 & 1\end{bmatrix}. \tag{4.29d}$$

The initial PDE-based thermal model governed by (4.19)–(4.20) has now been approximated by the above ODE-based model using the Chebyshev SGM.

Proposed 2D battery thermal model - brief summary

In this thesis, we propose a computationally efficient 2D battery thermal model for cylindrical and pouch LiBs, which is developed based on the Chebyshev spectral Galerkin approach. The proposed thermal model is well-suited for online thermal performance optimisation thanks to its ability to independently control the the tab and surface cooling channels of the battery. For brevity, we discuss only the model for the cylindrical cell. The original governing PDE for temperature $T(r,z,t)$ at time t and in the position (r,z) can be represented by the following 2D boundary value problem [71]

$$\rho C_p \frac{\partial T(r,z,t)}{\partial t} - k_r \frac{\partial^2 T(r,z,t)}{\partial r^2} - \frac{k_r \partial T(r,z,t)}{r \partial r} - k_z \frac{\partial^2 T(r,z,t)}{\partial z^2} = q(t) \tag{4.30}$$

subject to the non-homogeneous convection Robin boundary conditions given by

$$k_r \frac{\partial T}{\partial r} = h_s \left(T - T_{s,\infty}\right) \quad \text{at } r = R_{\text{out}}, \tag{4.31a}$$

$$k_r \frac{\partial T}{\partial r} = -h_c \left(T - T_{c,\infty}\right) \text{ at } r = R_{\text{in}}, \tag{4.31b}$$

$$k_z \frac{\partial T}{\partial z} = h_t \left(T - T_{t,\infty}\right) \quad \text{at } z = L, \tag{4.31c}$$

$$k_z \frac{\partial T}{\partial z} = -h_b \left(T - T_{b,\infty}\right) \text{ at } z = 0, \tag{4.31d}$$

where $r, z, R_{\text{in}}, R_{\text{out}}$, and L are the radial coordinates, axial coordinates, inner radius, outer radius, and height, respectively, of the cylindrical cell. The

subscripts s, c, t, and b denote the cell's surface, core, top, and bottom, respectively.

This 2D problem is more complex than the 1D problem discussed in Section 4.3. It involves cylindrical rather than Cartesian coordinates, requires non-dimensionalizing the physical domain into the range $[-1, 1]$, and the homogenization of the non-homogeneous boundary conditions is non-trivial due to the 2D nature of the problem. Furthermore, we aim to incorporate the boundary conditions into the control vector. Despite these complexities, the solution processes in both the 1D and 2D cases are fundamentally equivalent.

The final 2D battery thermal model can also be approximated by an ODE-based model in the state-space form of (4.27), and has the input vector

$$u(t) = \begin{bmatrix} u_s(t) & u_c(t) & u_t(t) & u_b(t) \end{bmatrix}^T, \tag{4.32}$$

where

$$u_s(t) = h_s(t)T_{s,\infty}(t), \qquad u_c(t) = -h_c(t)T_{c,\infty}(t), \tag{4.33a}$$

$$u_t(t) = h_t(t)T_{t,\infty}(t), \qquad u_b(t) = -h_b(t)T_{b,\infty}(t). \tag{4.33b}$$

Equations (4.32)–(4.33) are the cooling power applied to the surface, core, top and bottom sides of the cell. The above cooling power can be considered as the dynamic thermal system's input. Each of these inputs can be influenced by the coolant's temperature and flow rate.

CHAPTER 5

Model-based applications and battery control

The developed models for battery cells in the form of (4.27) can be effectively applied to various model-based applications, including rapid analysis of different cooling scenarios, real-time closed-loop temperature control, and thermal optimization of cell design. These aspects are thoroughly explored and detailed in the accompanying Paper B.

5.1 Model-based applications

Different cooling scenarios analysis

Selecting the most appropriate cooling scenario can significantly impact key thermal properties such as the average, maximum temperatures, and thermal gradients. The analyses are conducted under the heat generation profile of the worldwide harmonised light vehicle test procedure (WLTP) across the five cooling scenarios outlined in Table 5.1. The results indicate that bTC results in the highest average temperature while aTSC achieves the lowest average and maximum temperatures. Notwithstanding aTSC's advantage, it does not provide the lowest thermal gradient, which is instead achieved by btTC due

to its symmetric cooling from both the top and bottom sides of the cell.

Table 5.1: Cooling cases based on where cooling is imposed.

Cooling Scenario	Label
Surface cooling	SC
Bottom tab cooling	bTC
Bottom tab and surface cooling	bTSC
Bottom and top tabs cooling	btTC
All-tabs and surface cooling	aTSC

Furthermore, the cylindrical cell exhibits significantly higher thermal gradients in the radial direction compared to the axial direction, attributed to the lower radial thermal conductivity. This creates a bottleneck in heat transfer, resulting in the core temperature being the highest. To enhance cooling efficiency, increasing the cooling flow rate and utilizing battery materials with higher thermal conductivity are recommended. The analysis also reveals that no single cooling scenario consistently outperformed the others across all performance metrics, indicating that different scenarios may excel in specific aspects.

Evaluation and enhancement for cell design

The dimensions of a battery cell play a crucial role in determining its thermal properties, necessitating an understanding of geometric parameters for optimized cell design. By varying the length-to-radius ratio while maintaining a constant cell volume, it was found that a higher value of L/R_{out} typically leads to a more pronounced temperature rise and greater thermal gradients. Shorter and bulkier battery cells are generally more favourable than taller and slimmer designs. The analysis of current battery types in the market indicates that the 4680 cell type offers the best thermal performance across the five considered cooling scenarios.

Closed-loop temperature control

To address the performance trade-offs, a simple closed-loop temperature control strategy is implemented using multiple proportional-integral (PI) controllers as shown in Fig. 5.1. This strategy aims to maintain the average cell

temperature at a predefined set-point of 20 °C. The control scheme is tailored for each cooling scenario, allowing precise regulation of cooling power to specific sides of the cell. The results demonstrate that btTC best balances thermal gradients while under various C-rates.

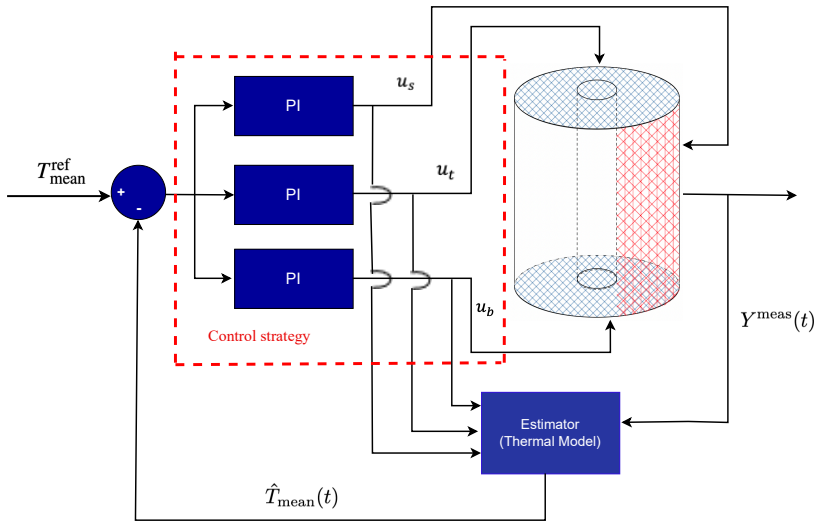

Figure 5.1: PI-based control scheme that tracks a given reference for the cylindrical cell's average temperature. $T^{\text{ref}}_{\text{mean}}$ and $\hat{T}_{\text{mean}}$ represent the set-point and estimate of the average temperature, respectively, and Y^{meas} is the cell's measurable outputs. The cooling power applied to the surface, top, and bottom, which are u_s, u_t, and u_b defined in (4.33), is regulated by their corresponding PI controllers. Their design parameters are set based on the specific cooling scenario. The blue and red-shaded areas of the plant represent the tab and surface cooling channels, respectively.

5.2 Optimal battery tab and surface coolant split control scheme

In Section 1.3, we outlined that the project work packages are broadly classified into two main categories: battery thermal modelling and control. While the latter is ongoing, we provide some key highlights here.

This work formalizes the integration of tab and surface cooling strategies as an optimal control problem. Tab cooling offers the advantage of homogeneous cooling, reducing thermal gradients within the cell, while surface cooling achieves a lower average cell temperature due to the larger surface area available for heat dissipation. Each strategy possesses distinct advantages and limitations, necessitating an optimal combination to minimize both thermal gradients and average temperature.

To achieve this, the problem is solved in a receding horizon fashion using the model predictive control (MPC) framework, allowing for dynamic adjustments based on real-time data. The objective is to optimally distribute the coolant flow between the tabs and the surface of the cell to minimise the average temperature rise and thermal gradients of the battery cell under various operating conditions. Moreover, physical constraints such as battery dynamics, health, and safety are observed in satisfying the objectives.

Reference Control Architecture

The BTMS in EVs comprises a coolant circulation system, where a mixture of water and glycol, driven by a pump, flows through channels or pipes embedded within or adjacent to the high-voltage battery pack. Cooling plates and microchannels, attached either to the curved surface or base of cylindrical cells, and to the surface in the case of pouch and prismatic cells, facilitate heat absorption and removal. The heat absorbed by the coolant is then transferred to a heat exchanger, which dissipates it to the ambient air or a secondary cooling circuit, such as a heat pump.

Heat pumps [80] are considered state-of-the-art heat exchangers in the EV industry due to their high efficiency, exceeding 300% [81]. The green-dashed box in Fig. 5.2 shows the schematic of a heat pump. Operating on the principle of thermodynamic heat transfer, a heat pump utilizes a refrigeration cycle to either heat or cool a medium. In the cooling mode for the BTMS, heat is extracted from the battery coolant into the refrigerant in the chiller (evapora-

tor). Subsequently, the compressor increases the pressure and temperature of the refrigerant, transforming it into a high-pressure super-heated vapour. The hot refrigerant then flows to the radiator (condenser), where it releases heat to the outside environment with a new state of high-pressure cooled saturated liquid. Following this, the expansion valve reduces the pressure and temperature of the refrigerant, converting it back into a low-pressure, low-temperature mixed liquid and vapour, thereby completing the cycle.

The next generation of EV battery packs is positioned to embrace the so-called cell-to-pack technology [82], [83], offering increased volumetric energy density, enhanced charging speed, extended range, and reduced production costs. Cylindrical cells are the preferred choice for this advancement due to their compatibility with this integration approach. Notably, prominent EV manufacturers like Tesla, Lucid and Rivian already utilise cylindrical cells in their vehicle designs. Furthermore, industry giants such as BMW [84] and General Motors [85], [86] are considering a transition to cylindrical cells, indicating a broader trend towards this innovative technology. Consequently, the cooling strategy in this work is demonstrated for the cylindrical cell but can be adapted to other cell form factors.

Our proposed optimal coolant split control strategy can be realised by the active cooling architecture shown in the red-dashed box of Fig. 5.2. This distinctive architecture known as the integrated switched-battery cooling (ISBC) system in this work, requires three separate cooling channels, each targeting different parts of the cell; the curved surface, top, and bottom sides. For simplicity, we assume the coolant flows to the sides instantaneously, without any input delay. Additionally, a three-way solenoid valve [87], [88], actuated by direct current (DC)-DC power converters, is responsible for splitting the coolant flow among the three individual channels. A more detailed ISBC system is shown in Fig. 5.3. To achieve the desired thermal performance objectives, the vehicle control unit (MPC) generates modulating signals $u_{dc,\varphi}(t) \in [0, 1]$, where the subscript $\varphi \in \{s, t, b\}$, with s, t, and b denoting the surface, top, and bottom channels/sides, respectively. Subsequently, the modulating signals are fed into a pulse width modulator (PWM), which produces binary (unipolar) switching functions $s_\varphi(t) \in \{0, 1\}$ to activate transistors within each power converter controlling each channel. From the valve control viewpoint, the variables, $u_{dc,\varphi} \in \mathcal{U} \subseteq \mathcal{R}^n$, can be viewed as control knobs to generate valve voltages $V_{sv,\varphi}(t) \geq 0$.

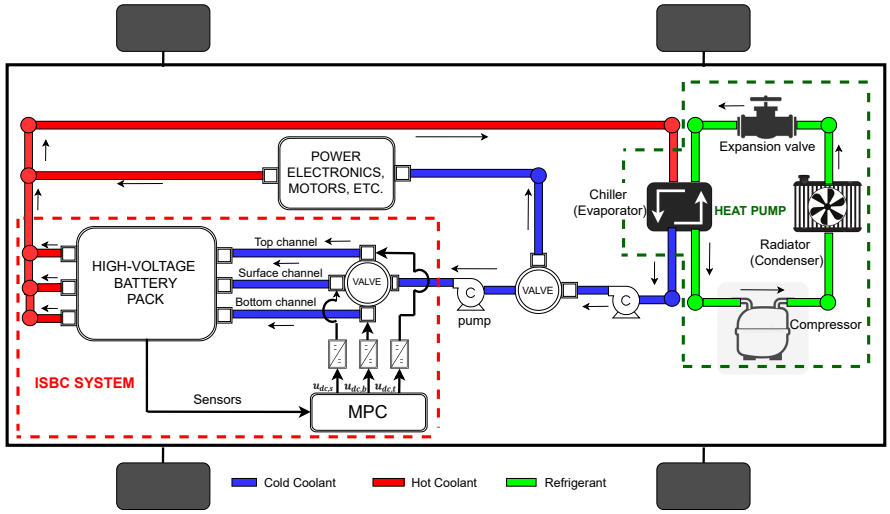

Figure 5.2: BTMS of an EV consisting of a heat pump with its refrigeration cycle (green-dashed box) and the proposed integrated switched-battery cooling (ISBC) system (red-dashed box). Centrifugal pumps drive the water and glycol mixture through the coolant circulation system. The red-coloured channels represent the hot coolant, the blue, the cooled coolant, and the green the refrigerant.

MPC formulation

To solve the optimal coolant split problem, it is essential to establish an MPC framework that includes all its critical components. This involves a detailed battery thermal model, a state estimator, a well-defined cost function, and constraints. The developed model in (4.27) is used as the predictive model within this framework. The proposed objective function at time step k is defined as follows,

$$J = \min_{u_{dc,\varphi}} \sum_{i=0}^{N-1} \left[w_1 \|\bar{T}_{\max}(k+i)\|^2_{Q_m} + w_2 \|\delta T(k+i)\|^2_{Q_\delta} + w_3 \|\Delta u_{dc,\varphi}(k+i)\|^2_R \right], \tag{5.1}$$

where $\|x\|^2_D := x^T D x$ denotes the weighted norm of vector x, $\{w_i \geq 0\,; i = 1, \cdots, 3\}$ represent trade-off weights, which are tuned to reflect the relative

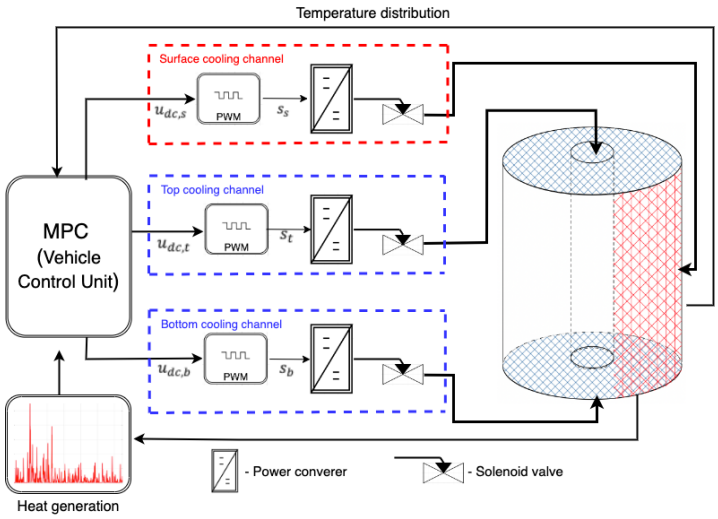

Figure 5.3: The proposed ISBC system provides a variable coolant flow to the surface, top, and bottom cooling channels by optimally actuating the valves controlling each channel. The ISBC consists of the battery, the model predictive controller, three power converters, a three-way solenoid valve, and sensors that measure the temperature distribution and heat generated by the cell.

importance of each objective.

$$\bar{T}_{\max}(k+i) = T_{\text{ref}}(k+i) - \bar{T}(k+i), \tag{5.2}$$

is the setpoint tracking error for the temperature rise of the cell, weighted by a semi-positive definite matrix, Q_m. T_{ref} is a predefined reference temperature, and $\bar{T}$ is the average temperature of the cell given by

$$\bar{T}(k+i) = \frac{1}{n}\sum_{j=1}^{n} T_j(k+i), \tag{5.3}$$

where T_j is the cell temperature distribution. $\delta T(k+i)$ is the thermal gradients in the cell, defined as the derivative of the temperature with respect to the radial and axial spatial variables r and z,

$$\delta T(k+i) = \frac{d(T_j(k+i))}{d\gamma}, \quad \text{where}, \gamma \in \{r, z\}. \tag{5.4}$$

This term is weighted by a semi-positive definite matrix, Q_δ. The slew rate,

$$\Delta u_{dc,\varphi}(k+i) = u_{dc,\varphi}(k+i+1) - u_{dc,\varphi}(k+i), \tag{5.5}$$

is the rate of change of control effort, penalised by the positive definite matrix R.

The first term aims to keep the cell in an optimal working range, which is essential for extending its overall lifetime. The second provides an enabling environment for the cell to age homogeneously as current density inhomogeneities and temperature hotspots in the cell which be minimised. In addition, temperature strains and stresses in any spatial direction will be reduced. It is desirable to achieve our objectives with minimum control effort and that is handled by the last term. Additionally, rapid voltage and current transitions can lead to switching losses and electrical stress on the ISBC components, causing insulation breakdown, wear and tear, and fatigue. The last term ensures smooth switching of the converter leading to the extension of the ISBC's lifetime. We also note that (5.1) is subject to the thermal system's dynamics, initial conditions, and physical constraints of the ISBC system.

Evaluation setup of optimal control scheme

We evaluate the effectiveness of the optimal coolant split scheme against state-of-the-art cooling methods used in EVs. Cylindrical battery cells are typically cooled either along their lateral surface (side) or their base, but rarely both simultaneously. These two conventional cooling approaches serve as benchmarks for comparison with our optimal scheme. The evaluation is conducted on a large format 45Ah lithium-ion-phosphate (LFP) battery with specifications similar to those described in attached papers A and B, under the original heat generation profile of the urban dynamometer driving schedule (UDDS) [89], which represents city driving conditions for light-duty vehicles. This comparison allows us to demonstrate the potential advantages of our optimized cooling approach in practical, real-world scenarios.

The cooling schemes under evaluation can be characterized by their active control inputs. The optimal coolant split scheme utilizes all three control inputs simultaneously; surface ($u_{dc,s}$), top ($u_{dc,t}$), and bottom ($u_{dc,b}$), all of which are actively controlled by the MPC. In contrast, the MPC in the side cooling scheme actuates only $u_{dc,s}$, while both $u_{dc,t}$ and $u_{dc,b}$ remain inactive.

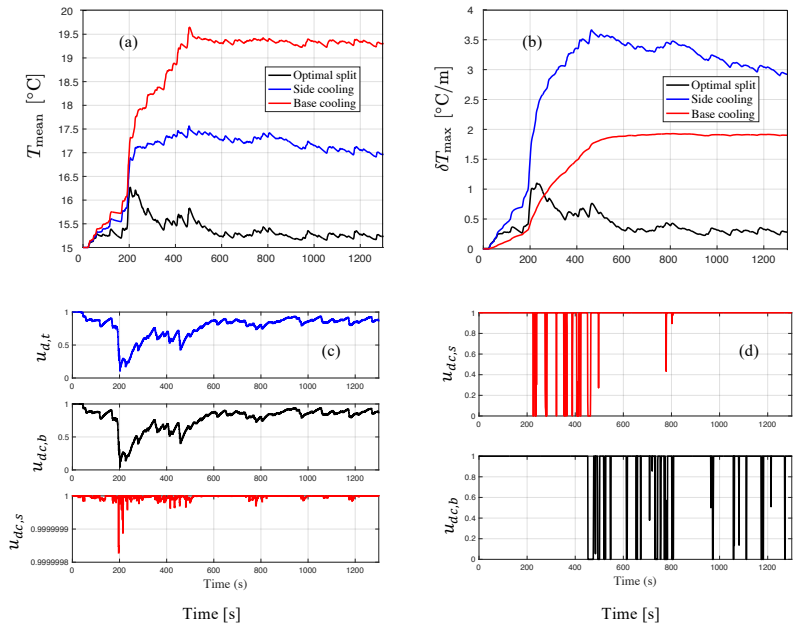

Figure 5.4: Results of the optimal coolant split scheme and its benchmarks. (a) Mean temperature, T_{mean}. (b) Max thermal gradients, $\delta T_{\max}$. (c) Control inputs, $u_{dc,\varphi}, \varphi \in \{s, t, b\}$, of optimal coolant split. (d) Control inputs of benchmarks. The plot in red represents the surface cooling control inputs, $u_{dc,s}$ and the black, base cooling, $u_{dc,b}$.

Similarly, only $u_{dc,b}$ is active in the base cooling while the other inputs are inactive.

Results and discussions

Even under this low heat generation, our proposed scheme demonstrates superior performance compared to conventional side and base cooling methods, as illustrated in Fig 5.4. With a prediction horizon of 10s, the results show significant improvements in both mean temperature and thermal gradients. Using the optimal scheme, the mean temperature is reduced to approximately 15.5 °C, compared to 17.5 °C with side cooling and 19.5 °C with base cooling,

as shown in Fig 5.4a. This represents a 21% reduction in mean temperature compared to base cooling and an 11.43% reduction compared to side cooling. Even more dramatic improvements are observed in thermal gradient results in Fig 5.4b. The optimal scheme reduces the maximum thermal gradients to about 0.25°C/m, compared to approximately 3°C/m for side cooling and 1.9°C/m for base cooling. This translates to a remarkable 92% reduction in thermal gradients compared to side cooling and an 87% reduction compared to base cooling.

Side cooling outperforms base cooling in reducing mean temperature due to the larger cell surface area utilized for heat dissipation. Conversely, base cooling is more effective in reducing thermal gradients because it allows all the rolled electrode layers in the cylindrical cell to be cooled simultaneously, resulting in a more homogeneous cooling effect. However, the optimal scheme presented here successfully combines and balances these somewhat conflicting objectives of minimizing both the average temperature rise and thermal gradients, for enhanced overall thermal performance. The control inputs shown in Figs 5.4c and d, demonstrate that the MPC respects the converter limits of $[0, 1]$, ensuring the practical applicability of the scheme.

This optimised cooling approach presented here has significant implications for EVs and battery applications in general. By maintaining lower and more uniform temperatures across the battery, it effectively slows down degradation processes and minimises hotspots that can accelerate battery wear and reduce lifespan. Additionally, minimizing thermal gradients reduces the risk of mechanical stress and potential thermal runaway hazards, ensuring safer battery operation.

CHAPTER 6

Summary of included papers

This chapter provides a summary of the included papers.

6.1 Paper A

Godwin K. Peprah, Torsten Wik, Yicun Huang, Faisal Altaf, Changfu Zou
Control-oriented 2D thermal modelling of cylindrical battery cells for optimal tab and surface cooling
Published in 2024 American Control Conference (ACC), Toronto, Canada
.

This work introduces a 2D thermal model for cylindrical LiBs, developed using the Chebyshev spectral-Galerkin method. The model's key innovation lies in its ability to independently control tab and surface cooling channels, enabling effective thermal performance optimization. Validated against a high-fidelity finite element model using real-world driving profiles, the research demonstrates that even a reduced-order model with one state can accurately predict spatially resolved temperature distribution throughout the cell. In ag-

gressive cooling scenarios, increasing the model order to nine states improves accuracy by about 84%. The study also reveals that while cooling all sides of the cell achieves the lowest average temperature rise, cooling only the top and bottom sides results in the lowest radial thermal gradient. Overall, the developed model proves to be a valuable tool for designing and implementing effective cooling strategies that minimize average temperature rise and thermal gradients in LiBs. The findings advocate for the model's integration into existing BMSs to enhance thermal management and optimize performance.

6.2 Paper B

Godwin K. Peprah, Yicun Huang, Torsten Wik, Faisal Altaf, Changfu Zou
Thermal modelling of battery cells for optimal tab and surface cooling control
Submitted to IEEE Transactions on Control Systems Technology.

This study develops a computationally efficient 2D thermal model for cylindrical and pouch cells, based on the Chebyshev spectral-Galerkin (CSG) method and pertinent model component decomposition. This yields a library of reduced-order battery thermal models, characterised by different number of states. These models allow for independent control of tab and surface cooling channels, optimizing thermal performance while accurately predicting spatially resolved temperature distributions with low errors. Notably, the one-state model demonstrates superior accuracy and efficiency compared to the widely used two-state thermal equivalent circuit (TEC) model, achieving a 28.7% reduction in computational time. The models have been validated against high-fidelity finite element models and real-world driving scenarios. Several cooling case studies reveal that exclusively cooling through the tabs on the top and bottom sides of cylindrical cells results in the lowest thermal gradients across various C-rates. Additionally, it shows that a lower length-to-radius ratio enhances thermal performance in cylindrical cells. These versatile models not only serve as a valuable tool for optimizing cooling strategies but also inform battery design, suggesting that commonly used cylindrical cell form factors may not be ideal for thermal management. Furthermore, the generality of the CSG framework can be extended beyond battery systems to other engineering fields involving partial differential equations with non-

homogeneous boundary conditions, such as heat transfer in electronics and stress analysis in complex materials.

CHAPTER 7

Concluding remarks and future work

This thesis has presented a thermal model and an optimal control scheme, in line with the research framework discussed in Section 1.3. The proposed thermal model and optimal control scheme represent a significant advancement in BTMS. By combining a computationally efficient battery thermal model with an optimal control strategy, this work addresses critical challenges in maintaining battery temperature within desired limits by balancing thermal gradients and average temperature rise.

The thermal model was developed based on the Chebyshev spectral-Galerkin method. This model is well-suited for online thermal performance optimisation, thanks to its ability to independently control signals to the battery's tab and surface cooling channels, while accurately predicting multi-spatial temperature distribution in the battery cell. The modelling framework has been presented here for both cylindrical and pouch cells and thoroughly evaluated on a large format cylindrical cell through various combinations of tab and surface cooling cases under real-world vehicle driving profiles. Additionally, the generality of the proposed modelling framework extends beyond battery systems. Its application extends to a wide range of systems governed by PDEs with non-homogenous boundary conditions. This versatility of the framework

in handling various geometries and boundary conditions makes it a powerful tool across multiple engineering disciplines.

The thesis also demonstrated that the novel model can readily replace existing TEC models in commercial BMS applications, for enhanced safety and lifetime applications. This stems from the developed model's computational efficiency, coupled with higher accuracy compared to its TEC counterpart.

Through various case studies, the model's utility in the design optimization of battery cells was showcased. Using the cylindrical cell as an example, findings revealed that a larger radius relative to the length of the cell is favourable for enhanced thermal performance. This observation suggests that typical cylindrical cell form factors prevalent in today's market, may not be ideally suited for thermal management. Given these insights, battery manufacturers and designers can make more informed decisions about cell geometry, potentially leading to significant improvements in thermal performance.

Future extensions

This thesis has laid a solid foundation for advanced battery thermal management. Future work will focus on several key areas, which include but are not limited to the

- systematic investigation of the control problem under various real-world battery usage conditions, explicitly studying the cost (degradation) associated with the control scheme,
- development of a closed-loop estimator with fast convergence and high robustness, leveraging the developed model,
- explicit addressing of model-plant mismatches and estimation errors to enhance control robustness, potentially through robust MPC techniques.
- extension of the model to pack level, allowing for more comprehensive thermal management in large-scale battery systems,
- modelling of the coolant dynamics to further refine the thermal management strategy, and
- conducting experimental tests and demonstrations to validate the model and control scheme in real-world conditions.

By addressing these areas, more efficient, safer, and long-lasting battery systems that can be applied across a wide gamut of applications, from EVs to grid-scale energy storage, to mention but a few, can be developed.

References

[1] M. Collins, R. Knutti, J. Arblaster, *et al.*, "Long-term climate change: Projections, commitments and irreversibility," 2013.

[2] Iiyama Miyuki, *Global temperatures in april 2024*, https://www.jircas.go.jp/en/program/proc/blog/20240515, Accessed: 2024-08-13.

[3] D. Wuebbles, D. Fahey, K. Hibbard, D. Dokken, B. Stewart, and T. Maycock, "Us global change research program," *Climate Science Special Report: Fourth National Climate Assessment*, vol. 1, p. 470, 2017.

[4] U. EPA, "Climate change in the united states: Benefits of global action. epa 430-r-15-001.," 2015.

[5] M. Vardy, M. Oppenheimer, N. K. Dubash, J. O'Reilly, and D. Jamieson, "The intergovernmental panel on climate change: Challenges and opportunities," *Annual Rev. of Environment and Resources*, vol. 42, no. 1, pp. 55–75, 2017.

[6] United Nations, "Fact sheet: Climate change," United Nations, Fact Sheet, 2021, Accessed: 2024-08-13.

[7] International Energy Agency, *Transport*, Accessed: August 13, 2024, 2023.

[8] S. Ma, M. Jiang, P. Tao, *et al.*, "Temperature effect and thermal impact in lithium-ion batteries: A review," *Progress in Natural Science: Materials Int.*, vol. 28, no. 6, pp. 653–666, 2018.

[9] J. Lin, X. Liu, S. Li, C. Zhang, and S. Yang, "A rev. on recent progress, challenges and perspective of battery thermal management system," *Int. J. Heat Mass Transf*, vol. 167, p. 120 834, 2021.

[10] P. R. Tete, M. M. Gupta, and S. S. Joshi, "Developments in battery thermal management systems for electric vehicles: A technical review," *J. Energy Storage*, vol. 35, p. 102 255, 2021.

[11] Y. Zhao, L. B. Diaz, Y. Patel, T. Zhang, and G. J. Offer, "How to cool lithium ion batteries: Optimising cell design using a thermally coupled model," *J. ochem. Soc.*, vol. 166, no. 13, A2849, 2019.

[12] I. A. Hunt, Y. Zhao, Y. Patel, and G. Offer, "Surface cooling causes accelerated degradation compared to tab cooling for lithium-ion pouch cells," *J. ochem. Soc.*, vol. 163, no. 9, A1846, 2016.

[13] Y. Zhao, Y. Patel, T. Zhang, and G. J. Offer, "Modeling the effects of thermal gradients induced by tab and surface cooling on lithium ion cell performance," *J. ochem. Soc.*, vol. 165, no. 13, A3169–A3178, 2018.

[14] S. Li, N. Kirkaldy, C. Zhang, *et al.*, "Optimal cell tab design and cooling strategy for cylindrical lithium-ion batteries," *J. Power Sources*, vol. 492, p. 229 594, 2021.

[15] C. Bolsinger and K. P. Birke, "Effect of different cooling configurations on thermal gradients inside cylindrical battery cells," *J. Energy Storage*, vol. 21, pp. 222–230, 2019.

[16] G. K. Peprah, F. Liberati, F. Altaf, G. Osei-Dadzie, A. Di Giorgio, and A. Pietrabissa, "Optimal load sharing in reconfigurable battery systems using an improved model predictive control method," in *IEEE Mediterranean Conf. Control and Automation*, IEEE, 2021, pp. 979–984.

[17] X. Lin, H. E. Perez, S. Mohan, *et al.*, "A lumped-parameter o-thermal model for cylindrical batteries," *J. Power Sources*, vol. 257, pp. 1–11, 2014.

[18] V. Srinivasan and C. Wang, "Analysis of ochemical and thermal behavior of li-ion cells," *J. ochem. Soc.*, vol. 150, no. 1, A98, 2002.

[19] J. Shen, T. Tang, and L.-L. Wang, *Spectral methods: algorithms, analysis and applications*. Springer Science & Business Media, 2011, vol. 41.

[20] L. N. Trefethen, *Spectral methods in MATLAB*. SIAM, 2000.

[21] R. R. Richardson, S. Zhao, and D. A. Howey, "On-board monitoring of 2-d spatially-resolved temperatures in cylindrical lithium-ion batteries: Part i. low-order thermal modelling," *J. Power Sources*, vol. 326, pp. 377–388, 2016.

[22] X. Hu, W. Liu, X. Lin, Y. Xie, A. M. Foley, and L. Hu, "A control-oriented othermal model for pouch-type electric vehicle batteries," *IEEE Trans. Power on.*, vol. 36, no. 5, pp. 5530–5544, 2020.

[23] E. J. Cairns, "Batteries, overview," *Encyclopedia of Energy*, vol. 1, pp. 117–126, 2004.

[24] S. Duehnen, J. Betz, M. Kolek, R. Schmuch, M. Winter, and T. Placke, "Toward green battery cells: Perspective on materials and technologies," *Small Methods*, vol. 4, no. 7, p. 2 000 039, 2020.

[25] G. Zubi, R. Dufo-López, M. Carvalho, and G. Pasaoglu, "The lithium-ion battery: State of the art and future perspectives," *Renewable and sustainable energy reviews*, vol. 89, pp. 292–308, 2018.

[26] J. B. Goodenough and Y. Kim, "Challenges for rechargeable li batteries," *Chemistry of materials*, vol. 22, no. 3, pp. 587–603, 2010.

[27] R. Xiong, "Battery management algorithm for electric vehicles," 2020.

[28] N. Nitta, F. Wu, J. T. Lee, and G. Yushin, "Li-ion battery materials: Present and future," *Materials today*, vol. 18, no. 5, pp. 252–264, 2015.

[29] E. Peled and S. Menkin, "Sei: Past, present and future," *J. ochem. Soc.*, vol. 164, no. 7, A1703, 2017.

[30] J. Zhu, M. S. D. Darma, M. Knapp, *et al.*, "Investigation of lithium-ion battery degradation mechanisms by combining differential voltage analysis and alternating current impedance," *J. Power Sources*, vol. 448, p. 227 575, 2020.

[31] ABC News. "Fire authorities warn of lithium-ion battery risks after two students narrowly escape melbourne fire." Accessed: 2024-08-14, Australian Broadcasting Corporation. (2024), [Online]. Available: https://www.abc.net.au/news/2024-04-18/lithium-battery-fire-phone-charger-students-building-carlton/103740394.

[32] Paul Crompton. "Ic scooter recall after battery fire causes deaths amid spate of two-wheeler fires in india." Accessed: 2024-08-14, Best Magazine. (2022), [Online]. Available: https://www.bestmag.co.uk/ic-scooter-recall-after-battery-fire-causes-deaths-amid-spate-of-two-wheeler-fires-in-inida/.

[33] A. Ohnsman, "Tesla's third model S fire brings call for U.S. inquiry," *Bloomberg*, 2013, Accessed: 2024-08-14.

[34] X. Feng, M. Ouyang, X. Liu, L. Lu, Y. Xia, and X. He, "Thermal runaway mechanism of lithium ion battery for electric vehicles: A review," *Energy storage materials*, vol. 10, pp. 246–267, 2018.

[35] N. Galushkin, N. Yazvinskaya, and D. Galushkin, "Mechanism of thermal runaway in lithium-ion cells," *J. ochem. Soc.*, vol. 165, no. 7, A1303, 2018.

[36] J. Jaguemont, L. Boulon, and Y. Dubé, "A comprehensive review of lithium-ion batteries used in hybrid and electric vehicles at cold temperatures," *Applied Energy*, vol. 164, pp. 99–114, 2016.

[37] X. Lin, K. Khosravinia, X. Hu, J. Li, and W. Lu, "Lithium plating mechanism, detection, and mitigation in lithium-ion batteries," *Progress in Energy and Combustion Science*, vol. 87, p. 100 953, 2021.

[38] C. Lefrou, P. Fabry, and J.-C. Poignet, *ochemistry: the basics, with examples*. Springer Science & Business Media, 2012.

[39] Brandon August, *Deep dive: Lithium ion batteries and heat*, https://www.recurrentauto.com/research/deep-dive-lithium-ion-batteries-and-heat, Accessed: 2024-08-15, 2023.

[40] N. A. Chaturvedi, R. Klein, J. Christensen, J. Ahmed, and A. Kojic, "Algorithms for advanced battery-management systems," *IEEE Control Systems magazine*, vol. 30, no. 3, pp. 49–68, 2010.

[41] H. A. Gabbar, A. M. Othman, and M. R. Abdussami, "Review of battery management systems (bms) development and industrial standards," *Technologies*, vol. 9, no. 2, p. 28, 2021.

[42] D. N. How, M. Hannan, M. H. Lipu, and P. J. Ker, "State of charge estimation for lithium-ion batteries using model-based and data-driven methods: A review," *Ieee Access*, vol. 7, pp. 136 116–136 136, 2019.

[43] S. Yang, C. Zhang, J. Jiang, W. Zhang, L. Zhang, and Y. Wang, "Review on state-of-health of lithium-ion batteries: Characterizations, estimations and applications," *J. Cleaner Production*, vol. 314, p. 128 015, 2021.

[44] A. Farmann and D. U. Sauer, "A comprehensive review of on-board state-of-available-power prediction techniques for lithium-ion batteries in electric vehicles," *Journal of Power Sources*, vol. 329, pp. 123–137, 2016.

[45] A. Škegro, C. Zou, and T. Wik, "Analysis of potential lifetime extension through dynamic battery reconfiguration," in *2023 25th European Conf. on Power onics and App.*, IEEE, 2023, pp. 1–11.

[46] X. Hu, K. Zhang, K. Liu, X. Lin, S. Dey, and S. Onori, "Advanced fault diagnosis for lithium-ion battery systems: A review of fault mechanisms, fault features, and diagnosis procedures," *IEEE Industrial onics Mag.*, vol. 14, no. 3, pp. 65–91, 2020.

[47] W. Wu, S. Wang, W. Wu, K. Chen, S. Hong, and Y. Lai, "A critical review of battery thermal performance and liquid based battery thermal management," *Energy conversion and management*, vol. 182, pp. 262–281, 2019.

[48] M. Lu, X. Zhang, J. Ji, X. Xu, and Y. Zhang, "Research progress on power battery cooling technology for electric vehicles," *J. Energy Storage*, vol. 27, p. 101 155, 2020.

[49] A. K. Thakur, R. Sathyamurthy, R. Velraj, *et al.*, "A state-of-the art review on advancing battery thermal management systems for fast-charging," *Applied Thermal Eng.*, vol. 226, p. 120 303, 2023.

[50] R. Mahamud and C. Park, "Reciprocating air flow for li-ion battery thermal management to improve temperature uniformity," *J. Power Sources*, vol. 196, no. 13, pp. 5685–5696, 2011.

[51] Q. Wang, B. Jiang, B. Li, and Y. Yan, "A critical review of thermal management models and solutions of lithium-ion batteries for the development of pure electric vehicles," *Renewable and Sustainable Energy Rev.*, vol. 64, pp. 106–128, 2016.

[52] G. Zhao, X. Wang, M. Negnevitsky, and C. Li, "An up-to-date review on the design improvement and optimization of the liquid-cooling battery thermal management system for electric vehicles," *Applied Thermal Eng.*, vol. 219, p. 119 626, 2023.

[53] J. Luo, D. Zou, Y. Wang, S. Wang, and L. Huang, "Battery thermal management systems (btms) based on phase change material (pcm): A comprehensive review," *Chemical Eng. J.*, vol. 430, p. 132 741, 2022.

[54] M. Pan and Y. Zhong, "Experimental and numerical investigation of a thermal management system for a li-ion battery pack using cutting copper fiber sintered skeleton/paraffin composite phase change materials," *Int. J. of Heat and Mass Transfer*, vol. 126, pp. 531–543, 2018.

[55] M. Bernagozzi, A. Georgoulas, N. Miche, and M. Marengo, "Heat pipes in battery thermal management systems for electric vehicles: A critical review," *Applied Thermal Eng.*, vol. 219, p. 119 495, 2023.

[56] J. Guo and F. Jiang, "A novel electric vehicle thermal management system based on cooling and heating of batteries by refrigerant," *Energy Conversion and Management*, vol. 237, p. 114 145, 2021.

[57] Y. Ji and C. Y. Wang, "Heating strategies for li-ion batteries operated from subzero temperatures," *ochimica Acta*, vol. 107, pp. 664–674, 2013.

[58] X. Hu, Y. Zheng, D. A. Howey, H. Perez, A. Foley, and M. Pecht, "Battery warm-up methodologies at subzero temperatures for automotive applications: Recent advances and perspectives," *Prog. in Energy and Combustion Science*, vol. 77, p. 100 806, 2020.

[59] C.-W. Zhang, K.-J. Xu, L.-Y. Li, M.-Z. Yang, H.-B. Gao, and S.-R. Chen, "Study on a battery thermal management system based on a thermoic effect," *Energies*, vol. 11, no. 2, p. 279, 2018.

[60] X.-G. Yang, T. Liu, and C.-Y. Wang, "Innovative heating of large-size automotive li-ion cells," *Journal of power sources*, vol. 342, pp. 598–604, 2017.

[61] J. Zhu, Z. Sun, X. Wei, and H. Dai, "An alternating current heating method for lithium-ion batteries from subzero temperatures," *International Journal of Energy Research*, vol. 40, no. 13, pp. 1869–1883, 2016.

[62] S. Tamilselvi, S. Gunasundari, N. Karuppiah, *et al.*, "A review on battery modelling techniques," *Sustainability*, vol. 13, no. 18, p. 10 042, 2021.

[63] V. Choudhari, A. Dhoble, and T. Sathe, "A review on effect of heat generation and various thermal management systems for lithium ion battery used for electric vehicle," *J. Energy Storage*, vol. 32, p. 101 729, 2020.

[64] L. Rao and J. Newman, "Heat-generation rate and general energy balance for insertion battery systems," *J. Electrochem. Soc.*, vol. 144, no. 8, p. 2697, 1997.

[65] J. Liu, S. Yadav, M. Salman, S. Chavan, and S. C. Kim, "Review of thermal coupled battery models and parameter identification for lithium-ion battery heat generation in ev battery thermal management system," *Int. J. of Heat and Mass Transfer*, vol. 218, p. 124 748, 2024.

[66] N. Sato, "Thermal behavior analysis of lithium-ion batteries for electric and hybrid vehicles," *J. Power sources*, vol. 99, no. 1-2, pp. 70–77, 2001.

[67] A. Urban, D.-H. Seo, and G. Ceder, "Computational understanding of li-ion batteries," *npj Computational Materials*, vol. 2, no. 1, pp. 1–13, 2016.

[68] K. Liu, Y. Gao, C. Zhu, *et al.*, "Electrochemical modeling and parameterization towards control-oriented management of lithium-ion batteries," *Control Eng. Practice*, vol. 124, p. 105 176, 2022.

[69] M. Alkhedher, A. B. Al Tahhan, J. Yousaf, M. Ghazal, R. Shahbazian-Yassar, and M. Ramadan, "Electrochemical and thermal modeling of lithium-ion batteries: A review of coupled approaches for improved thermal performance and safety lithium-ion batteries," *J. Energy Storage*, vol. 86, p. 111 172, 2024.

[70] H. Arunachalam, "A new multiscale modeling framework for lithium-ion battery dynamics: Theory, experiments, and comparative study with the doyle-fuller-newman model," Ph.D. dissertation, Clemson University, 2017.

[71] D. W. Hahn and M. N. Özisik, *Heat conduction*. John Wiley & Sons, 2012.

[72] E. R. Henquín and P. A. Aguirre, "Phenomenological model-based analysis of lithium batteries: Discharge, charge, relaxation times studies, and cycles analysis," *AIChE J.*, vol. 61, no. 1, pp. 90–102, 2015.

[73] W. Guo, Z. Sun, S. B. Vilsen, J. Meng, and D. I. Stroe, "Review of "grey box" lifetime modeling for lithium-ion battery: Combining physics and data-driven methods," *J. Energy Storage*, vol. 56, p. 105 992, 2022.

[74] S. Nejad, D. Gladwin, and D. Stone, "A systematic review of lumped-parameter equivalent circuit models for real-time estimation of lithium-ion battery states," *J. Power Sources*, vol. 316, pp. 183–196, 2016.

[75] J. Khalfi, N. Boumaaz, A. Soulmani, and E. M. Laadissi, "Box–jenkins black-box modeling of a lithium-ion battery cell based on automotive drive cycle data," *World EV J.*, vol. 12, no. 3, p. 102, 2021.

[76] C. Zou, A. Klintberg, Z. Wei, B. Fridholm, T. Wik, and B. Egardt, "Power capability prediction for lithium-ion batteries using economic nonlinear model predictive control," *J. Power Sources*, vol. 396, pp. 580–589, 2018.

[77] A. Quarteroni and A. Valli, *Numerical approximation of partial differential equations*. Springer Science & Business Media, 2008, vol. 23.

[78] J. N. Reddy, "An introduction to the finite element method," *New York*, vol. 27, p. 14, 1993.

[79] A. Quarteroni, F. Saleri, P. Gervasio, *et al.*, *Scientific computing with MATLAB and Octave*. Springer, 2006, vol. 3.

[80] N. Zhang, Y. Lu, Z. H. Ouderji, and Z. Yu, "Review of heat pump integrated energy systems for future zero-emission vehicles," *Energy*, vol. 273, p. 127 101, 2023.

[81] MIT Tech. Review, *Everything you need to know about the wild world of heat pumps*, https://www.technologyreview.com/2023/02/14/1068582/everything-you-need-to-know-about-heat-pumps/, Accessed: 2024-05-13, 2023.

[82] F. Pampel, S. Pischinger, and M. Teuber, "A systematic comparison of the packing density of battery cell-to-pack concepts at different degrees of implementation," *Results in Engineering*, vol. 13, p. 100 310, 2022.

[83] K. Shen, J. Sun, Y. Zheng, *et al.*, "A comprehensive analysis and experimental investigation for the thermal management of cell-to-pack battery system," *Applied Thermal Engineering*, vol. 211, p. 118 422, 2022.

[84] BMW Group, *More performance, CO2-reduced production, significantly lower costs: BMW group to use innovative round BMW battery cells in NEUE KLASSE from 2025 [press release]. München*, Accessed: 2024-05-14, 2022.

[85] General Motors, *GM and Samsung plan to invest to expand U.S. battery cell manufacturing*, https://news.gm.com/newsroom.detail.html/Pages/news/us/en/2023/apr/0426-samsungsdi.html, Accessed: 2024-05-13, 2023.

[86] S. Lee, *GM considering using cylinder batteries over pouch for EVs*, https://www.thelec.net/news/articleView.html?idxno=4376, Accessed: 2024-05-13, 2023.

[87] M. Taghizadeh, A. Ghaffari, and F. Najafi, "Modeling and identification of a solenoid valve for pwm control applications," *Comptes Rendus Mecanique*, vol. 337, no. 3, pp. 131–140, 2009.

[88] S. V. Angadi and R. L. Jackson, "A critical review on the solenoid valve reliability, performance and remaining useful life including its industrial applications," *Engineering Failure Analysis*, vol. 136, p. 106 231, 2022.

[89] L. Almatrafi, S. Badaam, and S. M. Qaisar, "Electric vehicle performance evaluation using udds, nycc and wltp drive cycles," in *2023 20th Learning and Technology Conference (L&T)*, IEEE, 2023, pp. 103–108.